Electronic Supplementary Material (ESI) for Journal of Materials Chemistry A.

Supplementary Information

A promising Metal-Organic Framework (MOF), MIL-96(Al) for CO_2 separation under wet conditions

Virginie Benoit,[a] Nicolas Chanut,[a] Renjith S. Pillai,[b] Marvin Benzaqui,[c,d] Isabelle Beurroies,[a] Sabine Devautour-Vinot,[b] Christian Serre,[c] Nathalie Steunou,[d] Guillaume Maurin,[b] Philip L. Llewellyn [*a]

[a.] *Aix-Marseille Univ, CNRS, MADIREL, Marseille, France.*

[b.] *Institut Charles Gerhardt Montpellier, Université de Montpellier, CNRS, ENSCM, Place E. Bataillon, 34095 Montpellier cedex 05, France.*

[c.] *PSL Res Univ, FRE CNRS 2000, Ecole Super Phys & Chim Ind Paris, Ecole Normale Super, Inst Mat Poreux Paris, 75005 Paris, France.*

[d.] *Institut Lavoisier de Versailles, UMR CNRS 8180, Université de Versailles St Quentin en Yvelines, Université Paris Saclay, 45 avenue des Etats-Unis 78035 Versailles Cedex. France.*

1. Molecular simulations details.

Table S1. LJ potential parameters for all atoms of the MIL-96(Al).

Atomic type	UFF	
	σ (Å)	ε /k_B (K)
Al	4.399	0.000
C	3.431	52.841
H	2.571	22.143
N	3.261	34.724
O	3.118	30.195

Table S2. Potential parameters and partial charges for the guests

Atomic type	σ (Å)	ε /k_B (K)	*q* (*e*)
O_e	3.1589	93.200	0.0000
H_e	0.00	0.000	0.5564
M_e	0.00	0.000	-1.1128
CH_4	3.730	148.000	0.0000
N2_N	3.310	36.000	-0.4820
N2_COM	0.00	0.000	0.9640
CO2_C	2.757	28.129	0.6512
CO2_O	3.033	80.507	-0.3256

2. Computational predictions

2.1. Single component H_2O, CO_2 and N_2 adsorption

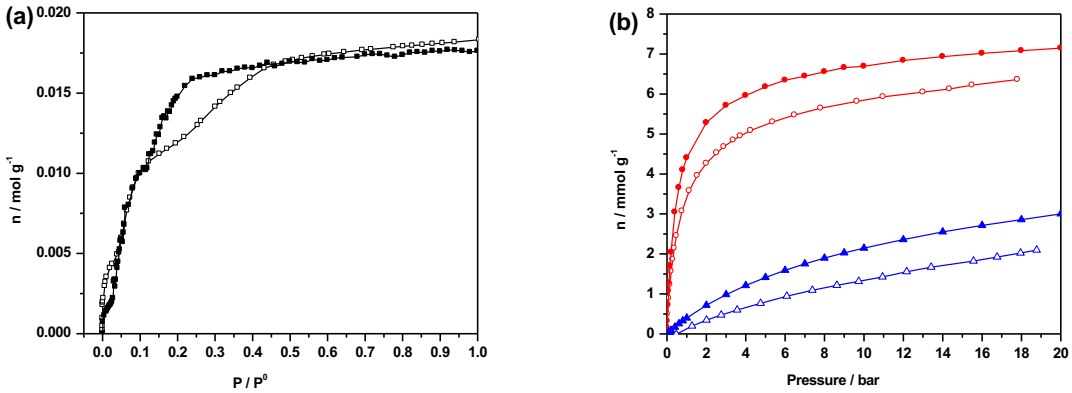

Figure S1. Comparison of the single component simulated (full symbols) and experimental (empty symbols) adsorption isotherms in MIL-96(Al) for H_2O (squares) at 298K (a) and CO_2 (squares) and N_2 (circles) at 303 K (b).

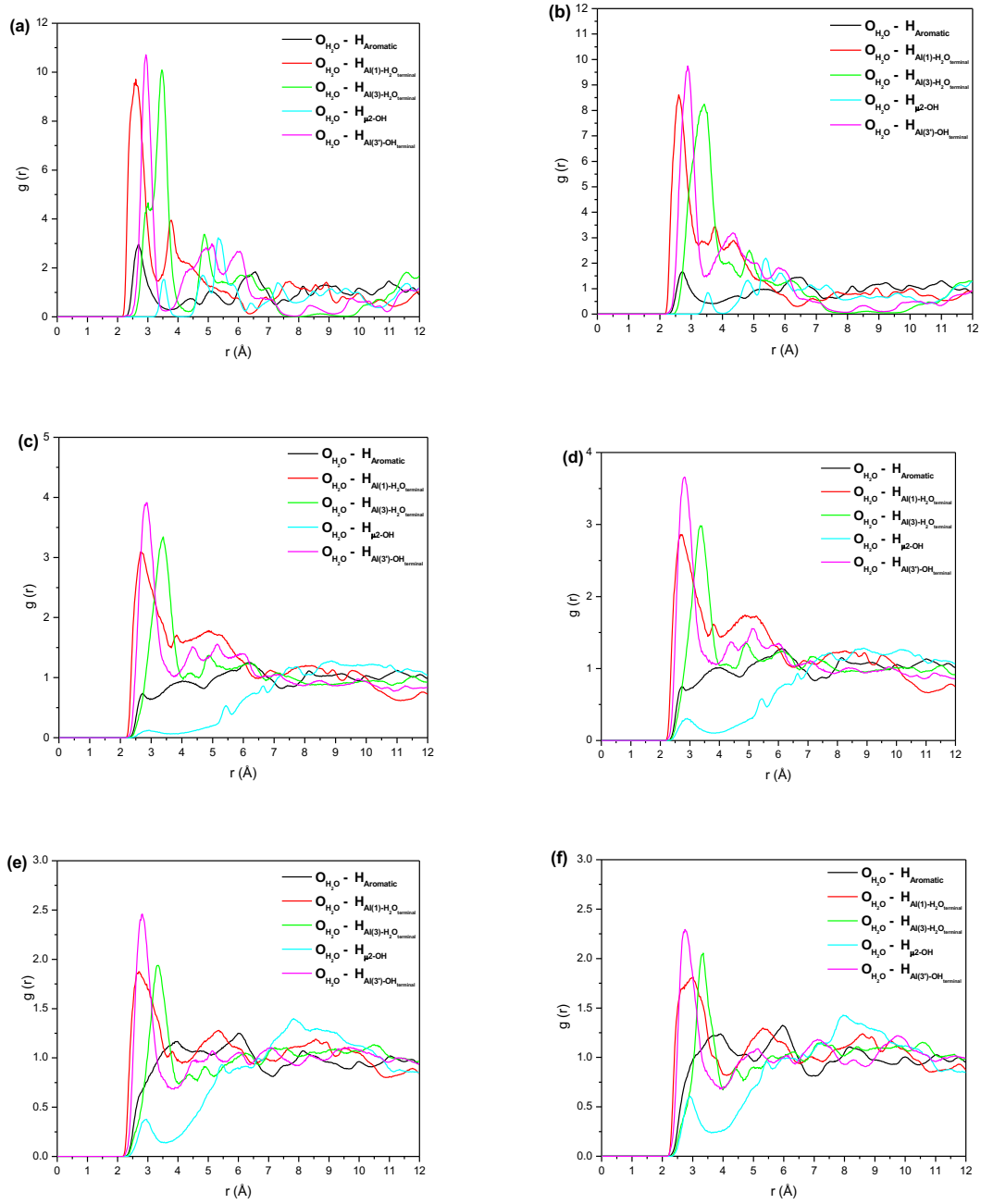

Figure S2: Radial Distribution Functions (RDF) between the oxygen atom of water (O_{H2O}) and all atoms of the MOF framework extracted from the GCMC simulations at 298 K in MIL-96(Al) at p/p°, 0.001 (a), 0.01(b), 0.05(c), 0.1 (d), 0.22 (e), and 1.0 (f).

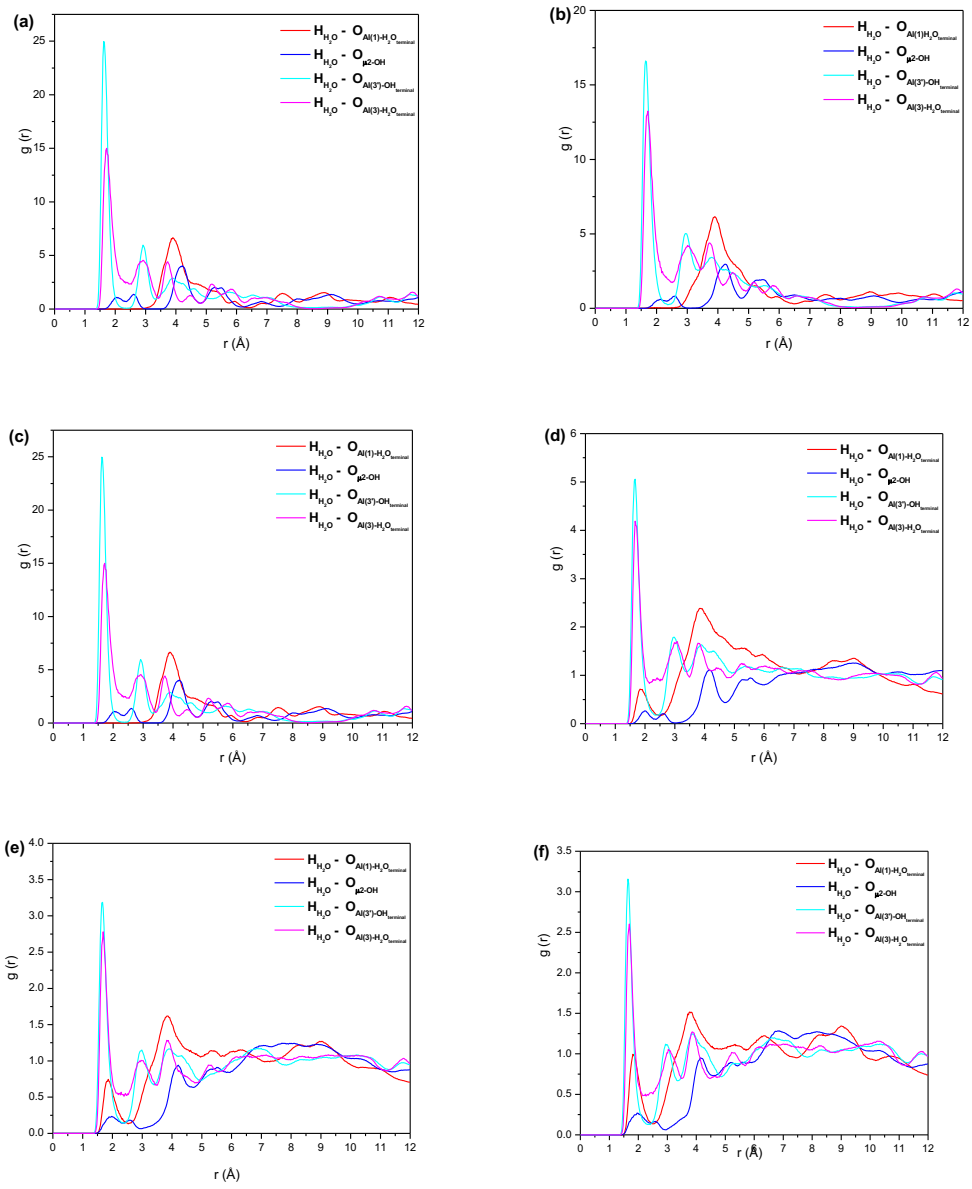

Figure S3: Radial Distribution Functions (RDF) between the hydrogen atom of water (H_{H2O}) that extracted from the GCMC simulations at 298 K in MIL-96(Al) at p/p°, 0.001 (a), 0.01(b), 0.05(c), 0.1 (d), 0.22 (e), and 1.0 (f).

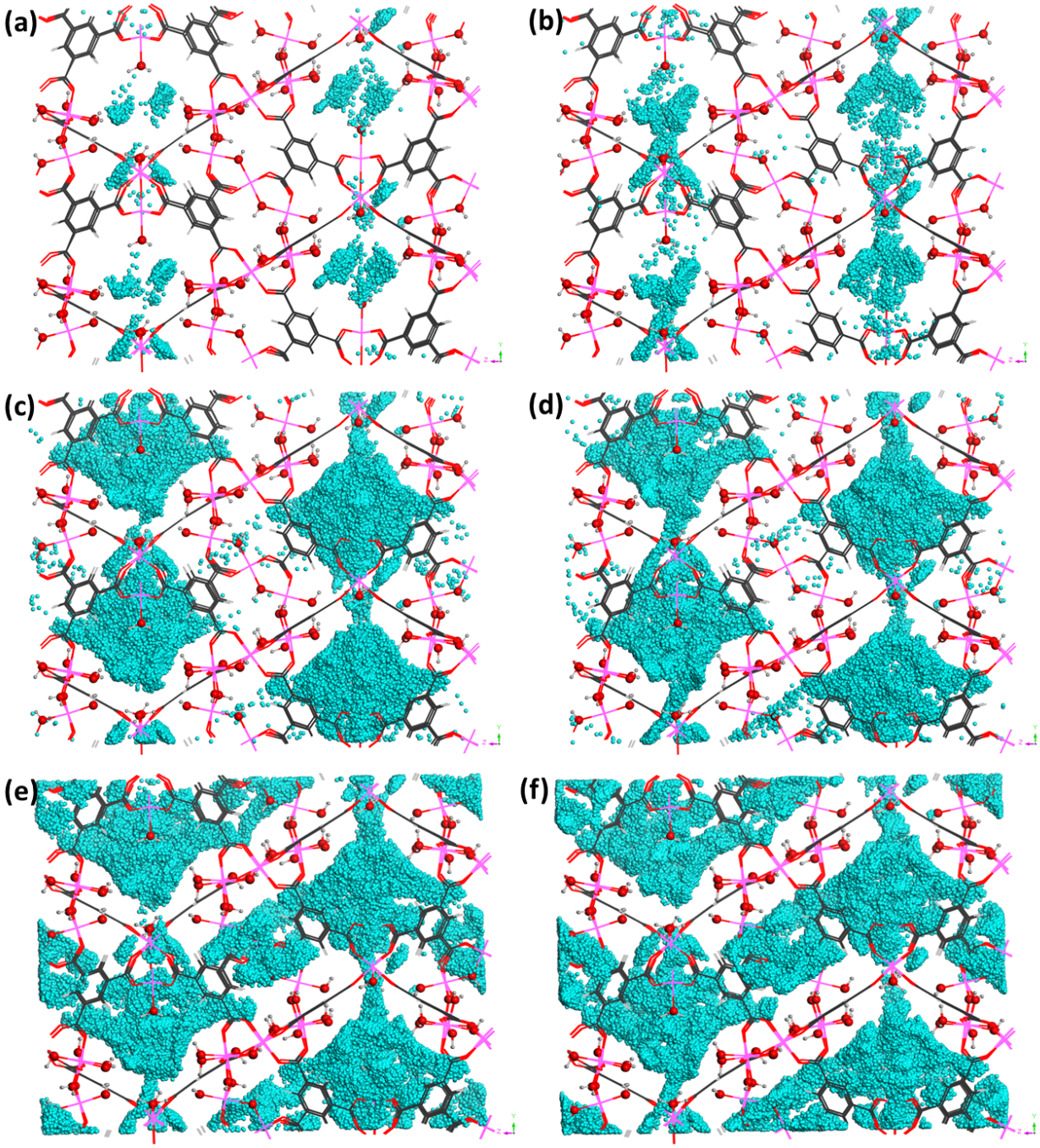

Figure S4: Maps of the occupied positions of H_2O (cyan) in 1000 equilibrated frames that extracted from the GCMC simulations at 298 K for MIL-96(Al) at p/p°, 0.001 (a), 0.01(b), 0.05(c), 0.1 (d), 0.12 (e), and 0.22 (f).

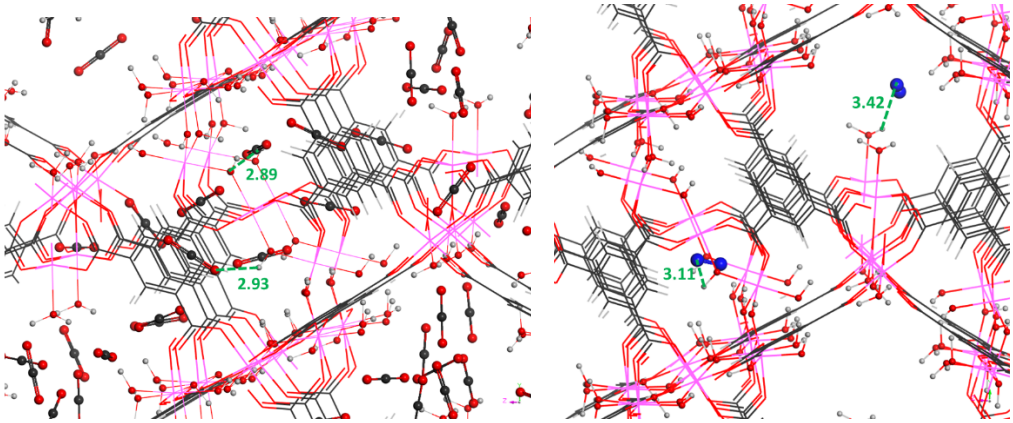

Figure S5. Local views of GCMC simulated arrangements of CO_2 (a) and N_2 (b) molecules in MIL-96(Al) at 303 K and 0.1 bar.

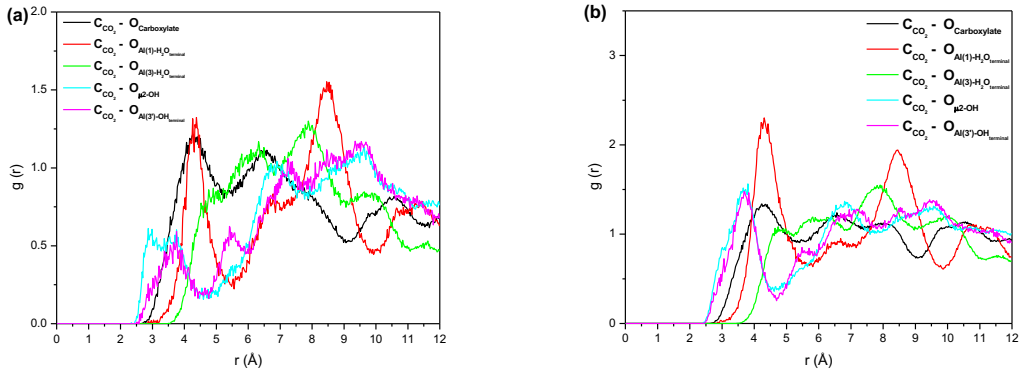

Figure S6: Radial Distribution Functions (RDF) between the Carbon of CO_2 (C_{CO2}) and all atoms of the MOF framework extracted from the GCMC simulations at 303 K in MIL-96(Al) at 0.01 bar (a) and 1.0 (b).

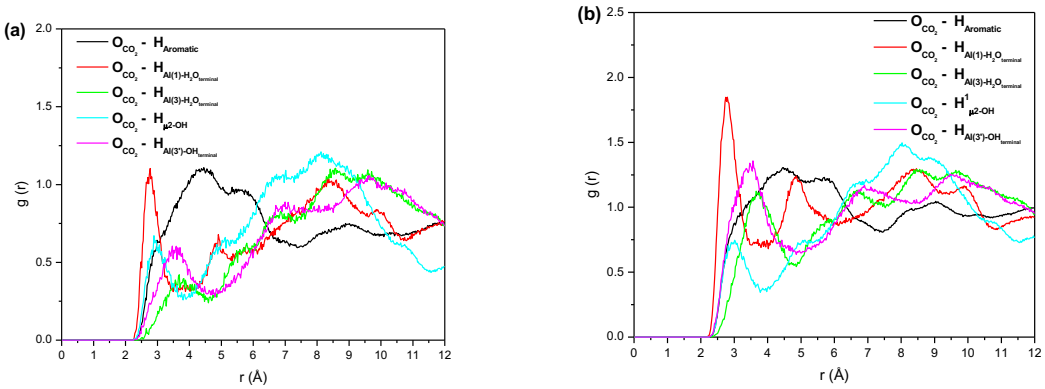

Figure S7: Radial Distribution Functions (RDF) between the oxygen in CO_2 (O_{CO2}) and all atoms of the MOF framework extracted from the GCMC simulations at 303 K in MIL-96(Al) at 0.01 bar (a) and 1.0 (b).

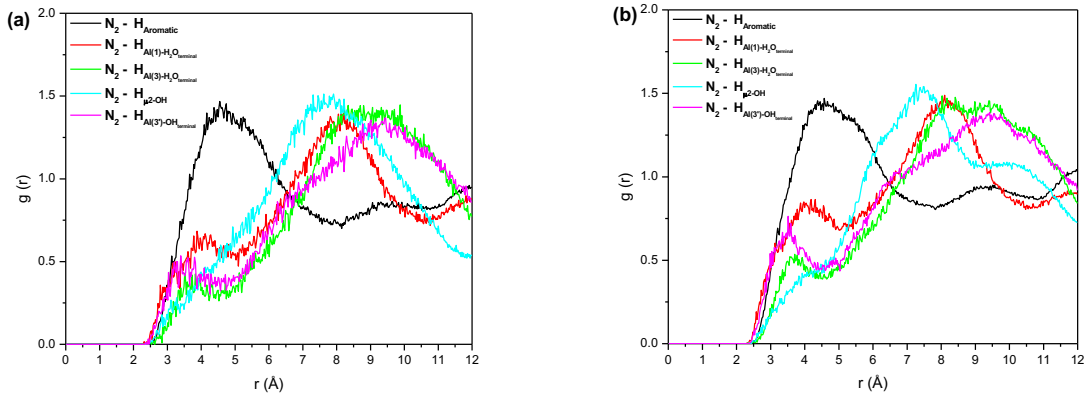

Figure S8: Radial Distribution Functions (RDF) between N_2 and all atoms of the MOF framework that extracted from the GCMC simulations at 303 K in MIL-96(Al) at 0.01 bar (a) and 1.0 (b).

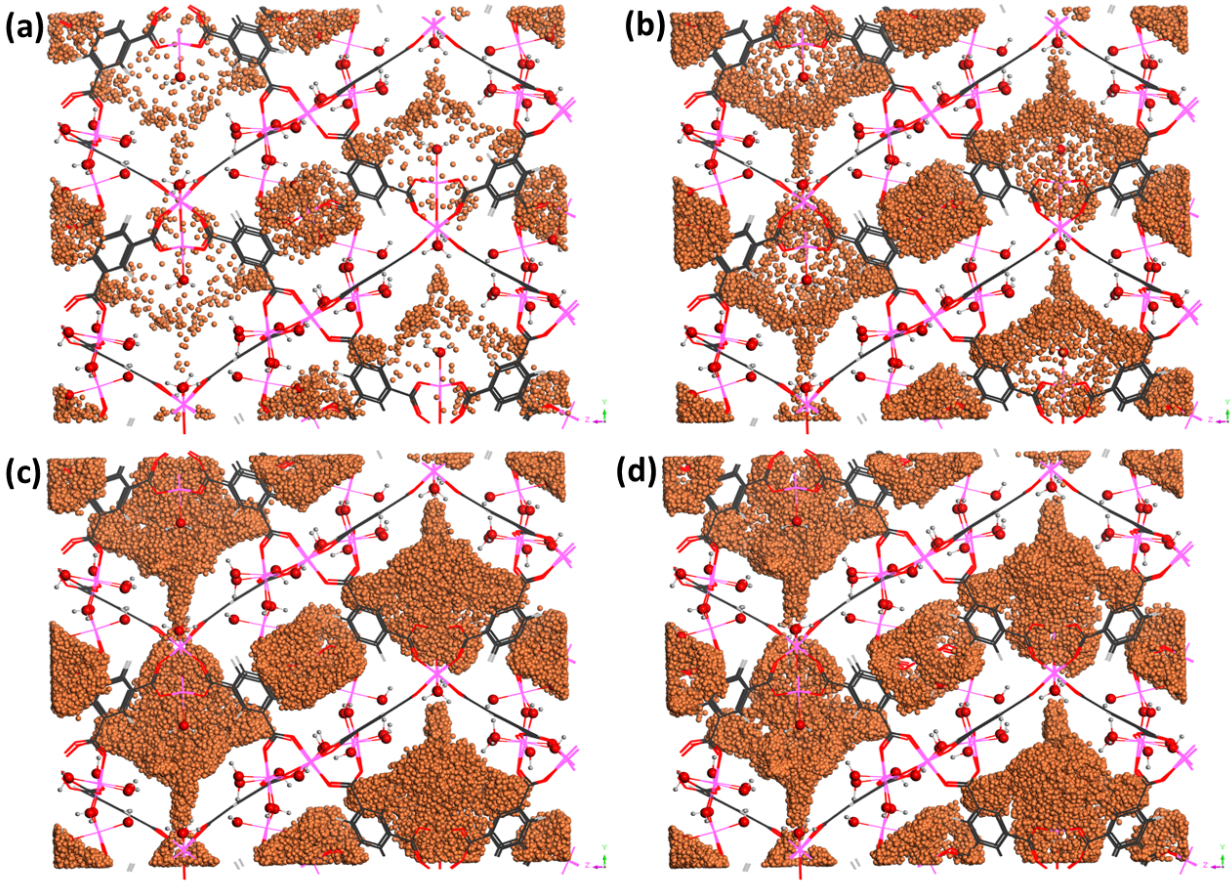

Figure S9: Maps of the occupied positions of CO_2 (orange) in 1000 equilibrated frames extracted from the GCMC simulations at 303 K for MIL-96(Al) at pressures: 0.01 bar (a), 0.1 bar (b), 1.0 bar (c), and 10.0 bar (d).

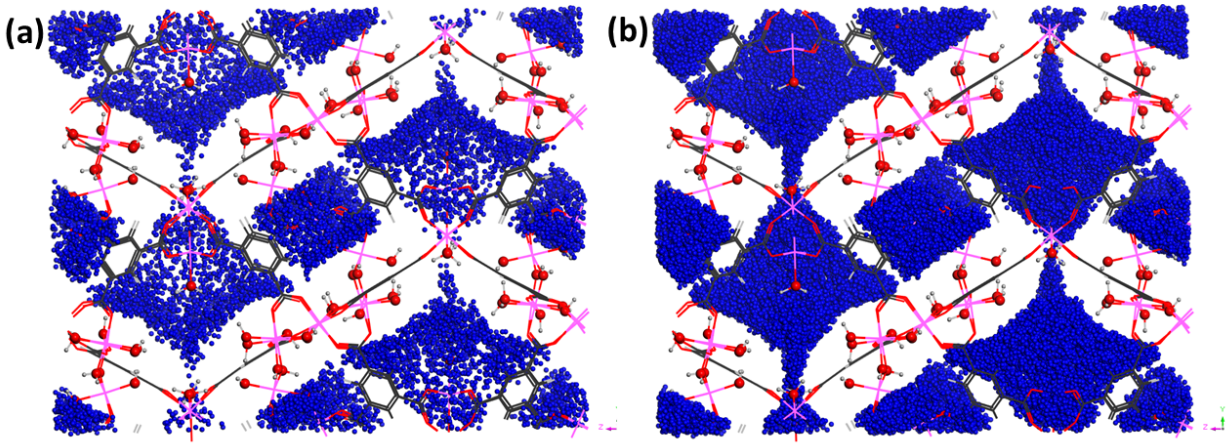

Figure S10: Maps of the occupied positions of N_2 (blue) in 1000 equilibrated frames extracted from the GCMC simulations at 303 K for MIL-96(Al) at pressures: 0.01 bar (a) and 10.0 (b).

2.2. Separation of CO_2/N_2 mixtures in presence and absence of humidity

In separation processes, a good indication of the separation ability consists of estimating the selectivity of a porous material. The selectivity (S) for CO_2 over N_2 is defined by the following expression: $S(CO_2/N_2) = \frac{(x_{CO_2} / x_{N_2})}{(y_{N_2} / y_{CO_2})}$ where x_{CO_2} and x_{N_2} are the mole fractions of CO_2 and N_2 in the adsorbed phase, respectively, while y_{CO_2} and y_{N_2} are the mole fractions of CO_2 and N_2 in the bulk gas phase, respectively. The calculated selectivities for both CO_2/N_2 (molar ratio =20/80) are shown in Figure S12 as a function of the bulk pressure.

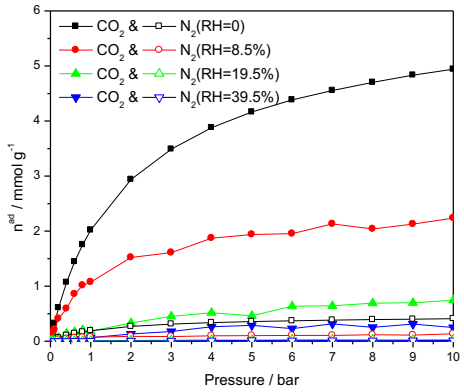

Figure S11. Simulated co-adsorption isotherm for CO_2 (closed symbols) and N_2 (open symbols) from their 20/80 molar ratio of binary gas mixture in presence of humidity, 0 % (square), 8.5% (circle), 19.5% (up-triangle) and 39.5% (down-triangle) as a function of the bulk pressure at 303 K.

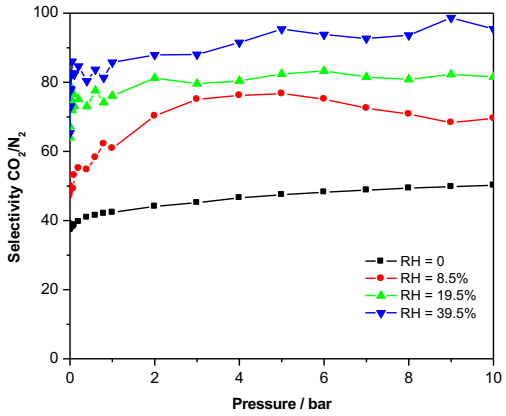

Figure S12. Simulated selectivities for CO_2/N_2 from their 20/80 molar ratio gas mixture in MIL-96(Al) as a function of the bulk pressure at 303 K and in presence of humidity (RH = 0 % (square), 8.5 % (circle), 19.5 % (up-triangle) and 39.5 % (down-triangle)).

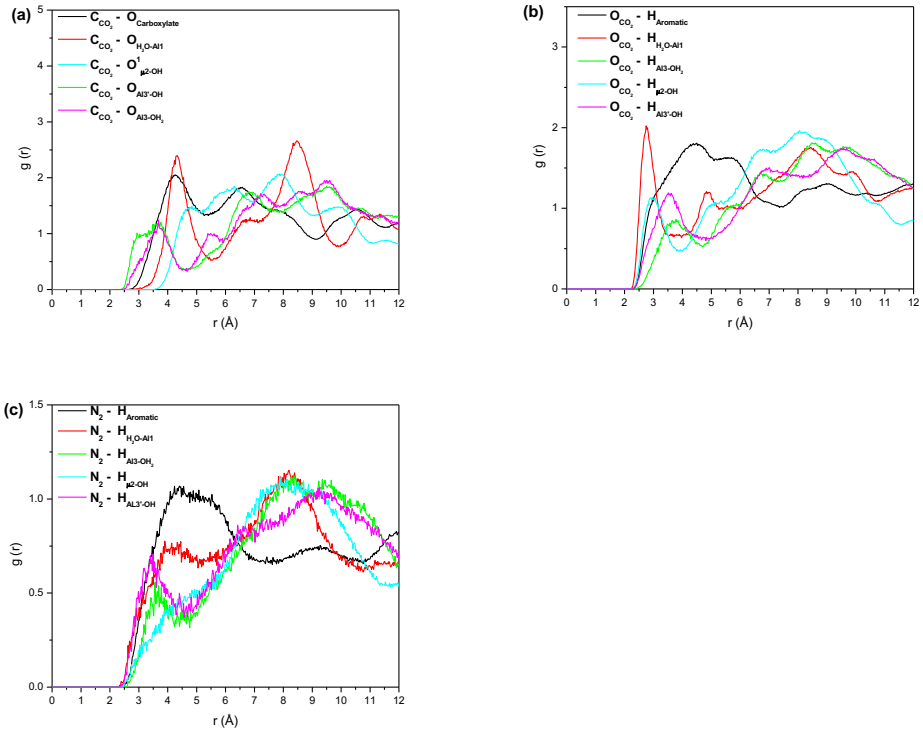

Figure S13: Radial Distribution Functions (RDF) between CO_2, C_{CO2} (a) and O_{CO2} (b), and N_2 (c) and all atoms of the MOF extracted from the GCMC simulations for co-adsorption of CO_2/N_2 = 20/80 in MIL-96(Al) at 303 K and 1.0 bar.

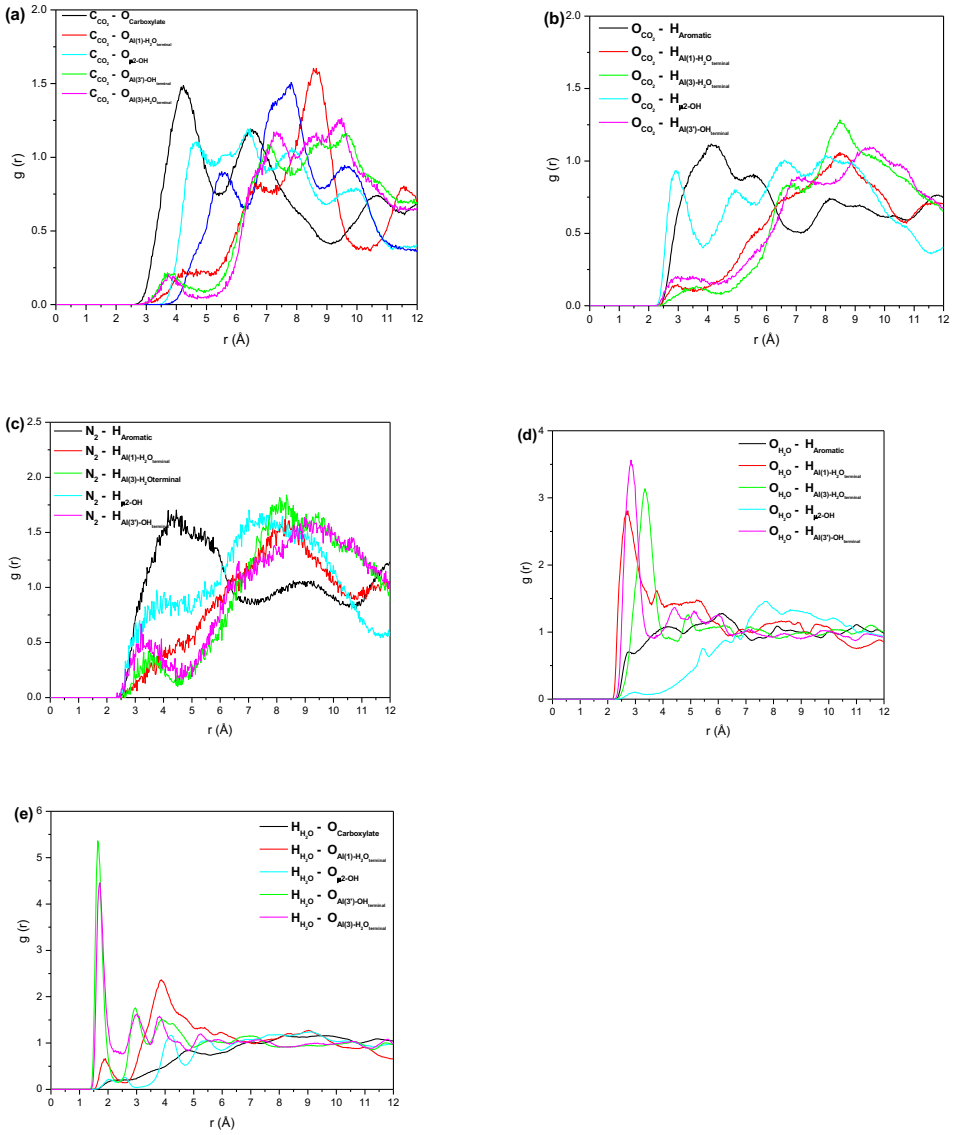

Figure S14: Radial Distribution Functions (RDF) between CO_2, C_{CO2} (a) and O_{CO2} (b), N_2 (c) and H_2O, O_{H2O} (d) and H_{H2O} (e) and all atoms of the MOF framework extracted from the GCMC simulations for co-adsorption of CO_2/N_2 = 20/80 in presence of humidity, RH=8.5%, in MIL-96(Al) at 303 K and 1.0 bar.

3. Complementary sample characterization

3.1 Textural parameters obtained from nitrogen physisorption at 77K

The accessible porosity of the MIL-96(Al) was probed by nitrogen gas adsorption at 77K using a Belsorb max apparatus. Prior to nitrogen adsorption, the MIL-96(Al) was outgassed at 150°C under secondary vacuum for 15h. From nitrogen adsorption isotherm at 77K, textural parameters were calculated such as apparent surface area, external surface and microporous volume.

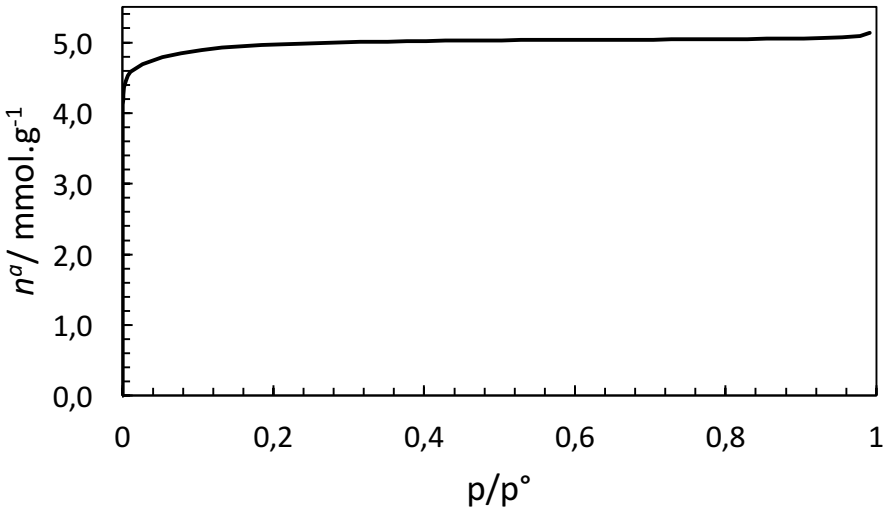

Figure S15 – Nitrogen adsorption isotherm at 77K obtained on MIL-96(Al)

Table S3. Textural parameters obtained from N_2 adsorption at 77K on the MIL-96(Al) and showing its microporous character.

MIL-96(Al)	S_{BET} 'apparent' (m^2/g)	S_{EXT} (m^2/g)	$V_{MICROPOROUS}$ (cm^3/g)
	448	1.2	0.16

3.2 Water isotherm on MIL-96(Al) at 298K

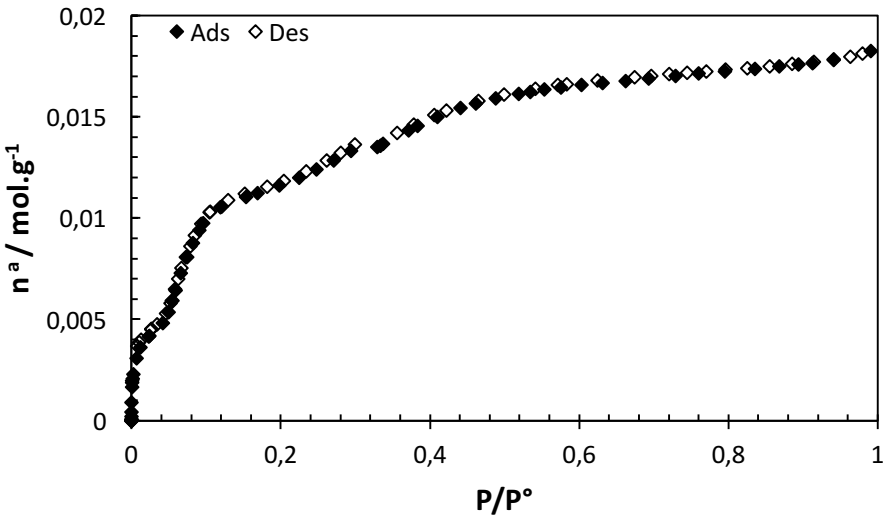

Figure S16. Water adsorption (fully lozenge) and desorption (empty lozenge) isotherms obtained at 298K on the MIL-96(Al)

4. Complementary results concerning static adsorption experiments at 303K

4.1. CO_2 adsorption isotherms and corresponding enthalpies of adsorption

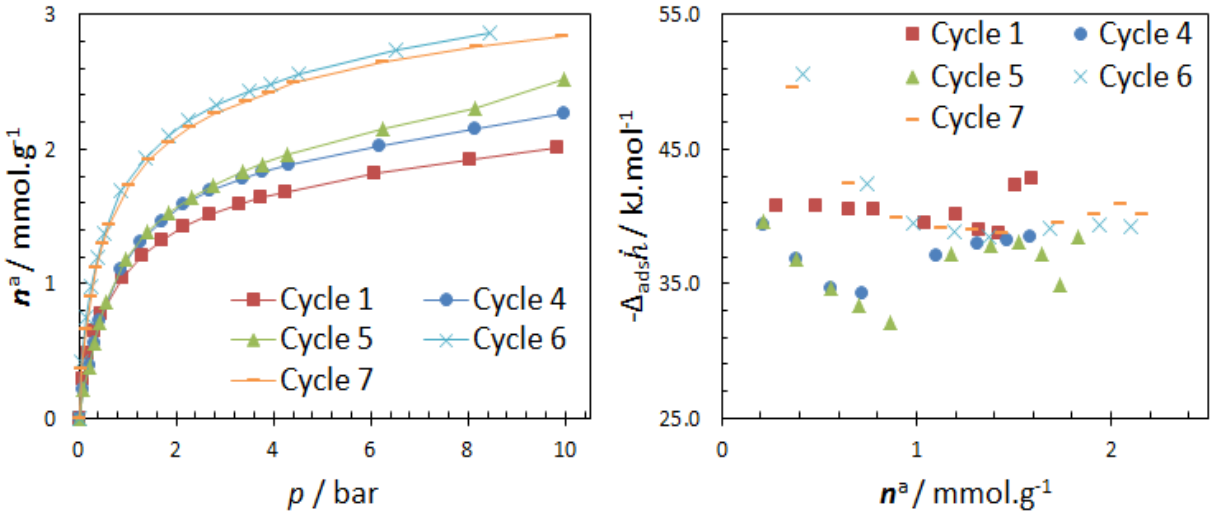

Figure S17 – CO_2 adsorption isotherms (left) and adsorption enthalpy profiles (right) obtained from cycling on the pre-humidified MIL-96(Al)

Table S4. Henry's law constant calculated at low surface coverage for CO_2 adsorption cycles: 1, 4, 6 from the MIL-96(Al) pre-humidified state and compared to these obtained on the MIL-96(Al) outgassed.

Cycle	1	4	6	Outgassed state
K_H – CO_2 / mmol.bar^{-1}.g^{-1}	5.05	6.34	10.26	17

5. Dynamic measurements to measure CO_2 uptakes in the presence of controlled relative humidity

5.1 Experimental set-up

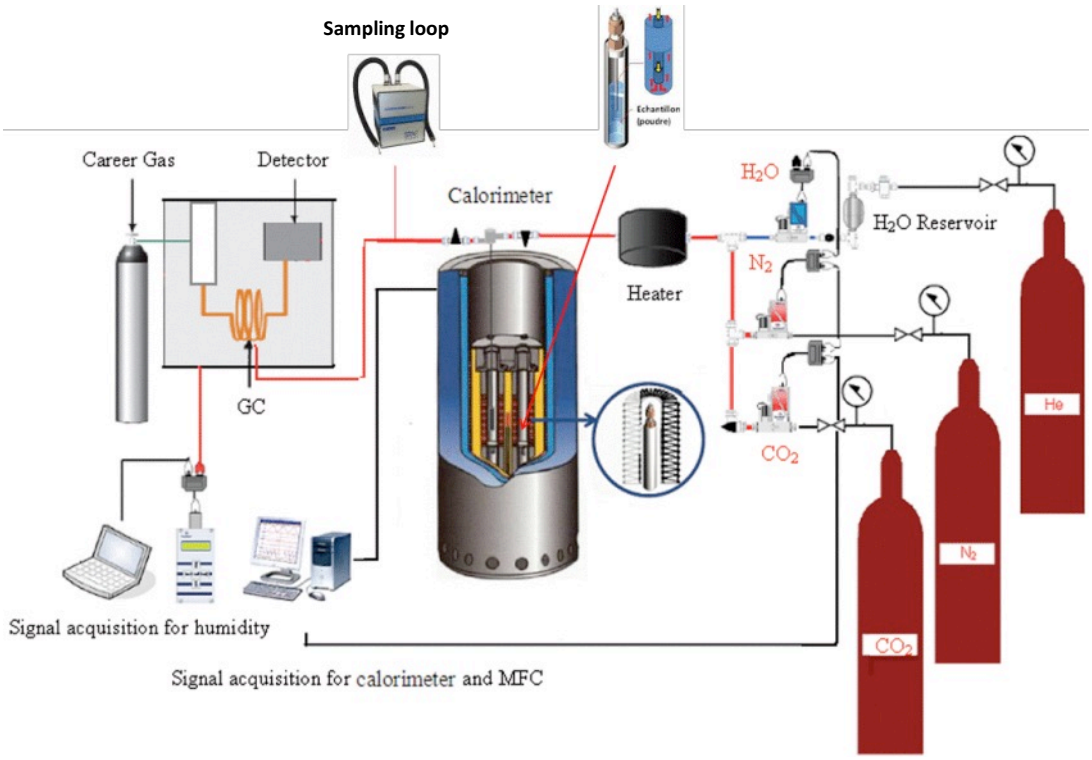

Figure S18. Schematic diagram of the flow adsorption microcalorimetry setup used to study the impact of water vapour during CO_2 adsorption on porous solids

Figure S18 shows a schematic diagram of the system used in our experiment: a Tian-Calvet type microcalorimeter and a gas chromatograph (GC6890N, Agilent) were coupled to simultaneously measure differential enthalpies of gas adsorption and CO_2 breakthrough curves. This rig was designed to operate in a dynamic mode at ambient temperature and at atmospheric pressure over a wide range of humidity. The system allowed 2 types of binary adsorption experiments (N_2/CO_2) either under dry conditions or under H_2O vapour. A central manual valve allowed a switching of the system from the dry mode to the wet mode. The sample was pre-treated directly inside the sample cell under nitrogen flow at the selected temperature. After activation, the sample was kept under continuous N_2 flow until thermal equilibrium was achieved. Then, gases (N_2, CO_2) and/or water vapour were flowed into the system, the proportion of each gas in the mixture being controlled by using mass flow controllers (MFC). In order to obtain a homogeneous mixture of gas, the flow rate of carrier gas (N_2) was 10 times larger than that of the adsorbate (CO_2). The total flow rate was maintained at a constant rate of 30 mLn/min. This part of the system is housed inside a thermostated chamber to keep the temperature constant. If an interaction between the gas mixture and the sample occurs, an energetic response is observed and recorded by the thermopiles of the microcalorimeter. The outlet gas mixture concentration from the cell is

then analyzed by the thermal conductivity detector (TCD) of the GC. In order to improve the accuracy of the measurement, a sampling loop has been added to the system in the course of this work. Indeed, when the adsorption process is fast, the time for the GC to analyze the outlet composition of the flue gas is too long which limits the number of points recorded to plot the breakthrough curve and therefore the accuracy of the measurement is lowered. The sampling loop collects and stores a sample of the flue gas (until 16 samples) at any programmed time and these collected samples are analyzed later by the GC. Thus, even if the adsorption process is fast, a large number of points can be used to plot the breakthrough curve.

5.2 Experimental protocols for the dynamic measurements

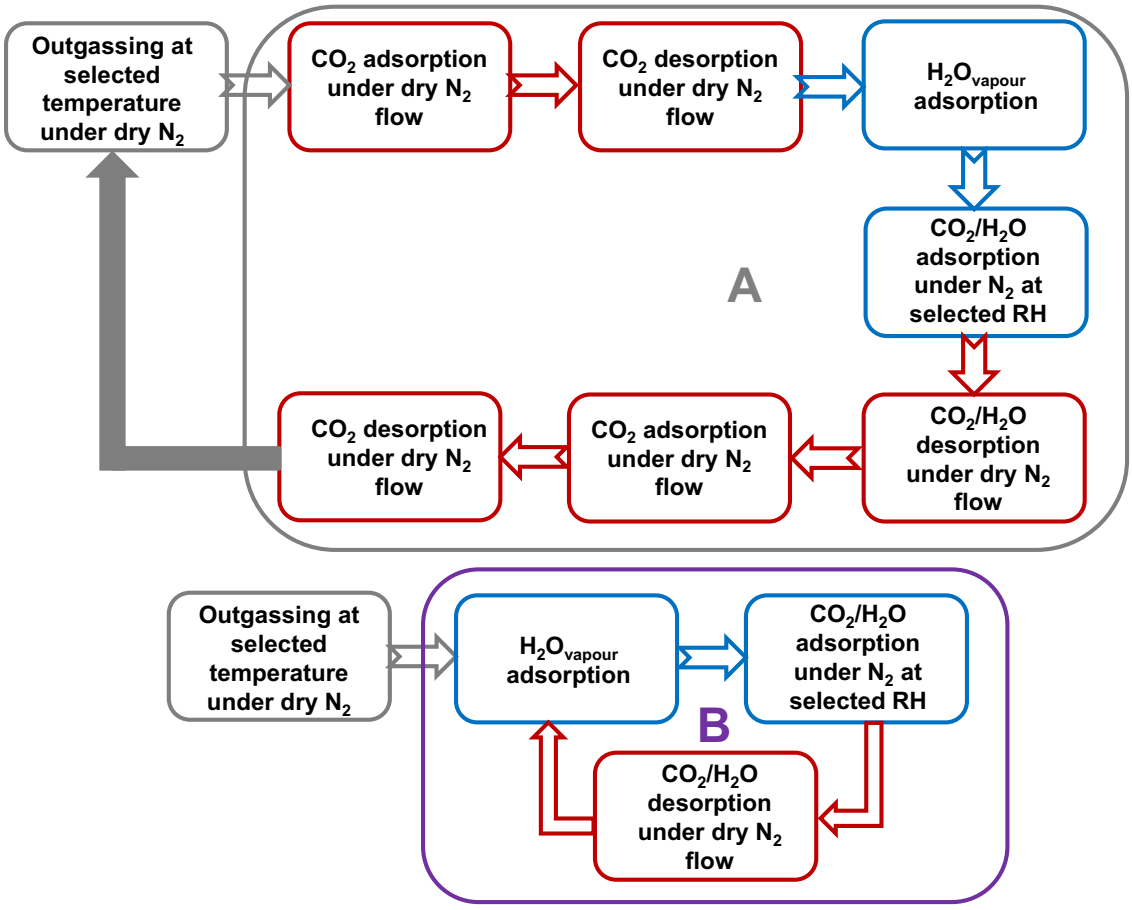

Figure S19 - Schematic representation of the different protocols used to evaluate adsorbents for post-combustion CO_2 capture in wet conditions (A) and for cycling experiments in wet conditions (B). Red frames correspond to the step performed in the dry mode of the system while blue frames correspond to the step performed in the wet mode of the system.

5.3 Complementary results from the dynamic CO_2 adsorption experiments

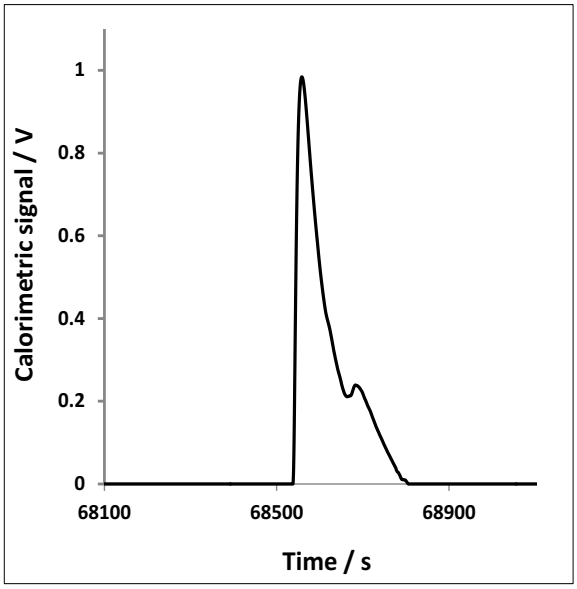

Figure S20. Unusual peak observed in the calorimetry signal which can be explained by the initial rapid (exothermic) adsorption of CO_2 followed by some H_2O desorption (endothermic) giving the trough in the overall signal.

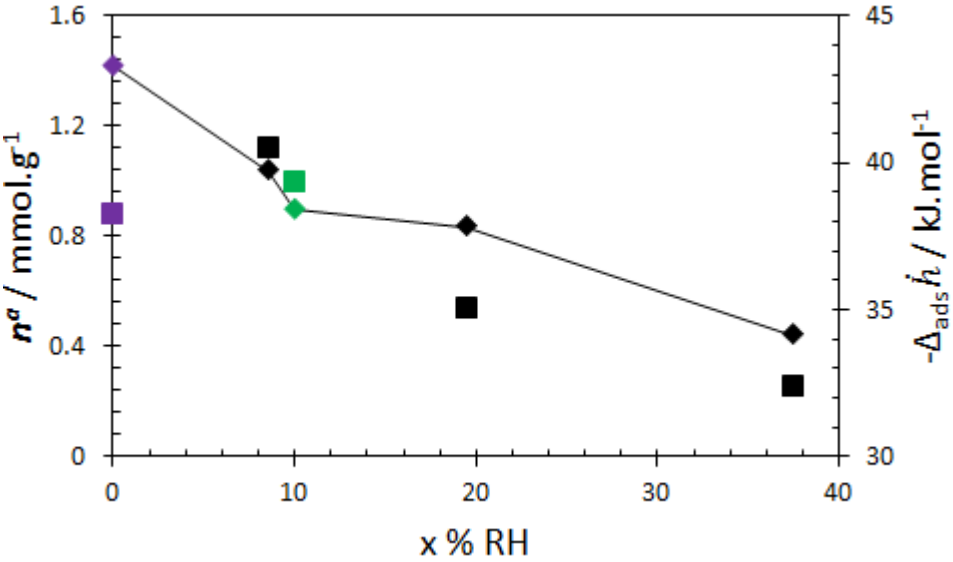

Figure S21 – CO_2 amount adsorbed (lozenge) and adsorption enthalpies (square) as function of relative humidity rate obtained from dynamic mode: 10 %, 20%, and 40% (black). After CO_2 adsorption under moisture conditions the MIL-96(Al) was dried in order to perform a new CO_2 adsorption cycle and uptake and enthalpy obtained are represented by purple points. The green points correspond to CO_2 uptake and enthalpy got from static mode after seven adsorption cycles on the pre-humidified MIL-96(Al).

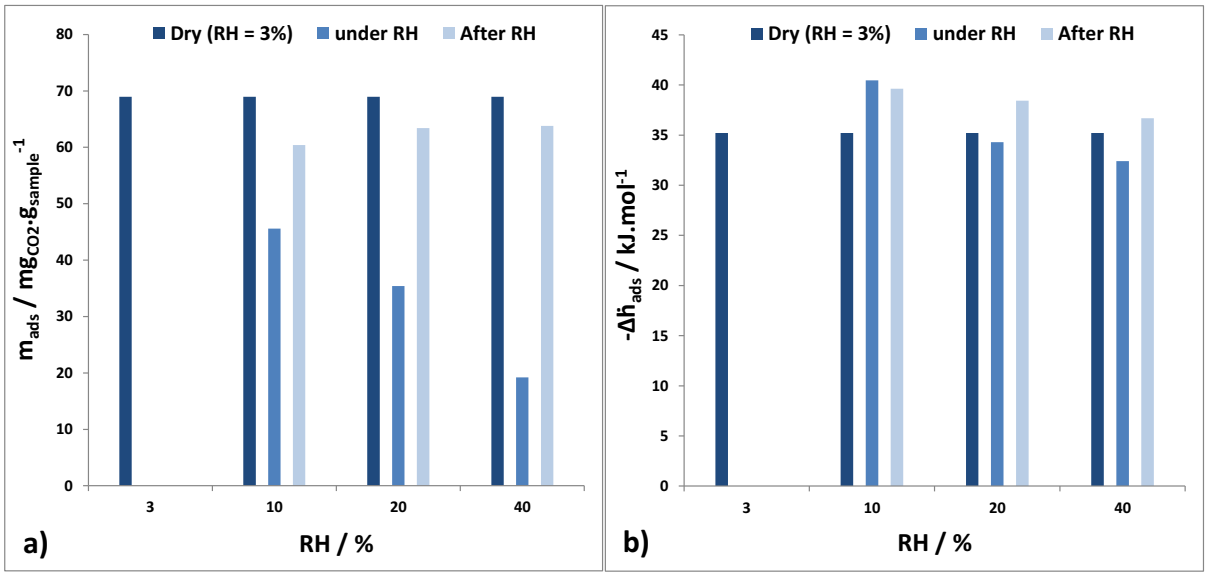

Figure S22 - CO_2 uptake on the MIL-96(Al) under dry conditions (RH = 3%), under RH = 10, 20 and 40% and after exposure to water vapour and b) the corresponding enthalpies of adsorption.

6. Further comparisons between samples

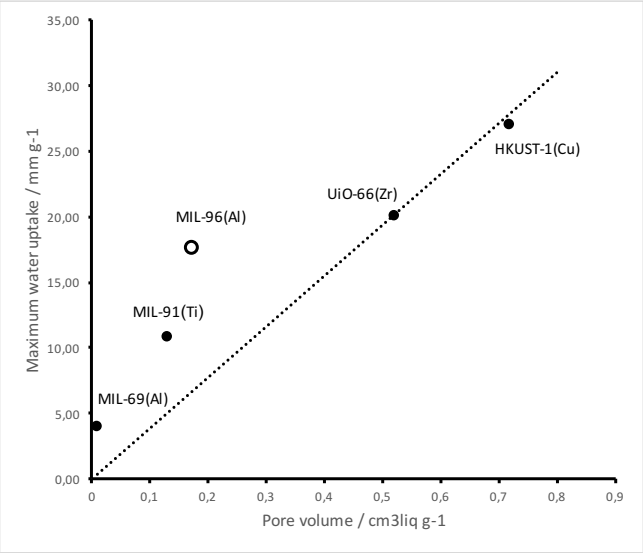

Figure S23. Correlation between maximum water uptake with respect to pore volume (calculated from N_2 physisorption at 77K) for several MOFs

Table S5. Henry's law constant calculated at low surface coverage for some MOFs having small pore size distribution.

Sample	MIL-69(Al)	MIL-91(Ti)	MIL-96(Al)	NH_2-MIL-53(Al)	MIL-53(Al)
Pore size distribution (Å)	3.1	3.9	4	6	8.5
K_H-H_2O (mol.g^{-1}.bar^{-1})	0.5	20.6	163	4.4	0.1

Table S6. Comparison of the selectivities for CO_2 / N_2 and CO_2 / CH_4 (2) Obtained from the open literature

Name	Mixture	%CO_2 in mixture	Selectivity	Calculation method	Ref
eea-MOF-4	CO_2/N_2	10	18	IAST	[1]
rtl-MOF-2	CO_2/N_2	10	38	IAST	[1]
SIFSIX-2Cu-i	CO_2/N_2	10	72	Measurement	[2]
Eu fcu-MOF	CO_2/N_2	10	82	IAST	[3]
SIFSIX-3-Cu	CO_2/N_2	10	15000	IAST	[4]
$Zn_4(pydc)_4(DMF)_2{\cdot}3DMF$	CO_2/N_2	15	42	IAST	[5]
UiO-66 (Zr) BTEC	CO_2/N_2	15	56	Measurement	[6]
Ni/DOBDC	CO_2/N_2	15	38	Measurement	[7]
USTA-16	CO_2/N_2	15	315	Measurement	[8]
MIL-91(Ti)	CO_2/N_2	15	150	IAST	[9]

Table S7. Initial enthalpies of adsorption for CO_2 as a function of CO2 uptake at low pressure, used to construct Figure 10.

Sample	Experimental conditions Temp/CO_2 partial pressure	CO_2 uptake	Enthalpy	Reference
MOF-74-Mg	296/ 0.1	5.36	47	[10]
MOF-74-Ni	296/ 0.1	2.74	41	[10]
MOF-74-Co	296/ 0.1	2.66	37	[10]
MOF-74-Zn	296/ 0.1	1.32	-	[10]
SIFSIX-3-Zn	298/ 0.15	2.43	45	[11]
SIFSIX-2-Cu-i	298/ 0.15	2.3	31.9	[11]
SIFSIX-2-Cu	298/ 0.15	0.36	22	[11]
$[Cu(bpy)_2SiF6)]$	298/ 0.2	1.1	-	[12]
$[Cu(bpy\text{-}1)_2SiF6)]$	298/ 0.15	0.84	27	[13]
$[Cu(bpy\text{-}2)_2SiF6)]$	298/ 0.15	0.52	21	[13]
UiO-66	298/ 0.1	0.67	25.5	[14]

[1] Z. Chen, K. Adil, L. J. Weseliński, Y. Belmabkhouta, M. Eddaoudi, *J. Mater. Chem. A*, **2015**, 3, 6276-6281.
[2] P. Nugent, Y. Belmabkhout, S. D. Burd, A. J. Cairns, R. Luebke, K. Forrest, T. Pham, S. Ma, B. Space, L. Wojtas, M. Eddaoudi, M.J. Zaworotko, *Nature*, **2013**, 495, 80–84.
[3] D.-X. Xue, Y. Belmabkhout, O. Shekhah, H. Jiang, K. Adil, A. J. Cairns, M. Eddaoudi, *J. Amer. Chem. Soc*., **2015**, 137, 5034-5040.
[4] O. Shekhah, Y. Belmabkhout, Z. Chen, V. Guillerm, A. Cairns, K. Adil, M. Eddaoudi, *Nat. Comms*., **2014**, 5, 4228.
[5] S. R. Ahrenholtz, C. Landaverde-Alvarado, M. Whiting, S. Lin, C. Slebodnick, E. Marand, A. J. Morris, *Inorg. Chem*., **2015**, 54(9), 4328-4336.
[6] Q. Yang, S. Vaesen, F. Ragon, A. D. Wiersum, D. Wu, A. Lago, T. Devic, C. Martineau, F. Taulelle, P. L. Llewellyn, H. Jobic, C. Zhong, C. Serre, G. De Weireld, G. Maurin, *Angew. Chem. Int. Ed*., **2013**, 52,
[7] J. Liu, J. Tian, P. K. Thallapally, B. P. McGrail, *J. Phys. Chem. C*, **2012**, 116(17):9575 – 9581.
[8] S. C. Xiang, Y. B. He, Z. J. Zhang, H. Wu, W. Zhou, R. Krishna and B. L. Chen, *Nat. Commun*., **2012**, 3, 954.
[9] V. Benoit, R. S. Pillai, A. Orsi, P. Normand, H. Jobic, F. Nouar, P. Billemont, E. Bloch, S. Bourrelly, T. Devic, P. A. Wright, G. de Weireld, C. Serre, G. Maurin and P. L. Llewellyn, *J. Mater. Chem. A*., **2016**, 4, 1383–1389
[10] S. R. Caskey, A. G. Wong-Foy, A. J. Matzger, *J. Amer. Chem. Soc.,* **2008**, 130, 33.
[11] P. Nugent, Y. Belmabkhout, S. D. Burd, A. J. Cairns,R. Luebke, K. Forrest, T. Pham, S. Ma, B.Space, L. Wojtas, M. Eddaoudi, M. J. Zaworotko, *Nature.* **2013**, 495, 80-84.
[12] K. A. Forrest, T. Pham, P. Nugent, S. D. Burd, A. Mullen, L. Wojtas, M. J. Zaworotko, B. Space, *Cryst. Growth Des.* **2013**, 13, 4542-4548.
[13] S. D. Burd, S. Ma, J. A. Perman, B. J. Sikora, R. Q. Snurr, P. K. Thallapally, J. Tian, L. Wojtas, M. J. Zaworotko, *J. Amer. Chem. Soc.* **2012**, 134, 3663-3666.
[14] Q. Wang, J. Bai , Z. Lu , Y. Pan , X. You, *Chem. Commun.* **2016**, 52, 443-452.